

Nuclear localized C9orf72 associated arginine containing dipeptides exhibit age-dependent toxicity in *C. elegans*

Paige Rudich¹, Carley Snoznik², Simon C. Watkins^{3,4}, John Monaghan², Udai Bhan Pandey^{2,5,6}, Todd Lamitina*,^{1,2,4}

¹Graduate Program in Cell Biology and Molecular Physiology, University of Pittsburgh Medical Center

²Division of Child Neurology, Department of Pediatrics, Children's Hospital of Pittsburgh, University of Pittsburgh Medical Center, Pittsburgh, PA, USA

³Center for Biologic Imaging, University of Pittsburgh School of Medicine

⁴Department of Cell Biology, University of Pittsburgh School of Medicine

⁵Department of Human Genetics, University of Pittsburgh Graduate School of Public Health, Pittsburgh, PA, USA

⁶Department of Neurology, University of Pittsburgh School of Medicine, Pittsburgh, PA, USA

*Address correspondence to Todd Lamitina, Ph.D., Children's Hospital of Pittsburgh of the University of Pittsburgh Medical Center, Departments of Pediatrics and Cell Biology, 4401 Penn Avenue, Rangos 7122, Pittsburgh, PA 15224, phone - (412) 692-9437; fax – (412) 641-1844; email - stl52@pitt.edu

© The Author 2017. Published by Oxford University Press.

This is an Open Access article distributed under the terms of the Creative Commons Attribution Non-Commercial License (<http://creativecommons.org/licenses/by-nc/4.0/>), which permits non-commercial re-use, distribution, and reproduction in any medium, provided the original work is properly cited. For commercial re-use, please contact journals.permissions@oup.com

Abstract

A hexanucleotide repeat expansion mutation in the C9orf72 gene represents a prevalent genetic cause of several neurodegenerative diseases, including amyotrophic lateral sclerosis (ALS) and frontotemporal dementia (FTD). Non-canonical translation of this repeat gives rise to several distinct dipeptide protein species that could play pathological roles in disease. Here, we show in the model system *C. elegans* that expression of the arginine-containing dipeptides, but not alanine-containing dipeptides, produces toxic phenotypes in multiple cellular contexts, including motor neurons. Expression of either (PR)₅₀ or (GR)₅₀ during development caused a highly penetrant developmental arrest, while post-developmental expression caused age-onset paralysis. Both (PR)₅₀- and (GR)₅₀-GFP tagged dipeptides were present in the nucleus and nuclear localization was necessary and sufficient for their toxicity. Using an inducible expression system, we discovered that age-onset phenotypes caused by (PR)₅₀ required both continual (PR)₅₀ expression and an aged cellular environment. The toxicity of (PR)₅₀ was modified by genetic mutations that uncouple physiological ageing from chronological ageing. However, these same mutations failed to modify the toxicity of (GR)₅₀, suggesting that (PR)₅₀ and (GR)₅₀ exert their toxicity through partially distinct mechanism(s). Changing the rate of physiological ageing also mitigates toxicity in other *C. elegans* models of ALS, suggesting that the (PR)₅₀ dipeptide might engage similar toxicity mechanisms as other ALS disease-causing proteins.

Introduction

Amyotrophic lateral sclerosis (ALS) and frontotemporal dementia (FTD) are devastating and currently incurable neurodegenerative disorders. Most cases of both ALS and FTD with known genetic etiology are caused by the expansion of an intronic GGGGCC (G_4C_2) hexanucleotide repeat in the chromosome 9 open reading frame 72 (C9orf72) gene (1, 2). Several mechanisms for why this repeat leads to disease have been proposed, including loss of C9orf72 function, nuclear G_4C_2 RNA foci formation, and abnormal translation of dipeptide repeat proteins (DPRs) (3). Recent work shows that C9orf72-associated DPRs accumulate in the spinal fluid of C9 ALS/FTD patients and can cause cell death in *in vitro* and *in vivo* settings (4-8). While this suggests an important role for DPRs in C9 ALS/FTD pathogenesis, analysis of post-mortem brain samples shows that DPRs are present at very low levels in brain regions that undergo the most severe neurodegeneration (i.e. spinal cord motor neurons), thus calling into question the relevance of DPR proteins in disease pathogenesis (9, 10). While this discrepancy could be due to a variety of factors (poor antibody detection of toxic species, loss of DPR-expressing neurons in end-stage samples), understanding the relationship between the individual DPRs and neurodegeneration in a variety of settings will be necessary to parse out the role of the DPRs in the development of C9orf72-associated diseases.

Translation of the intronic G_4C_2 repeat occurs through a process termed repeat-associated non-AUG dependent (RAN) translation (11). RAN translation of the G_4C_2 repeats can give rise to five distinct DPRs – proline-alanine (PA), glycine-alanine (GA), proline-arginine (PR), glycine-proline (GP), and glycine-arginine (GR). While PA, GP, and GA are not thought to cause significant toxicity, PR and to a lesser extent GR have

been shown to be toxic in yeast, *Drosophila*, and mammalian cell models (6-8). Recent studies implicate several pathways in the toxicity of the PR RAN dipeptide (8, 12, 13). Given that both ALS and FTD exhibit age-related onset and that age-related phenotypes are not easily modeled in cellular systems, organismal models are needed to examine the role of cell non-autonomous ageing regulatory pathways on the onset and severity of DPR toxicity. In this study, we establish *C. elegans* as a new model for investigating DPR toxicity mechanisms *in vivo*. We expressed codon-optimized transgenes for four DPRs (GA, PA, GR, PR) and characterized their toxicity and expression patterns. We found that 1) arginine-containing DPRs exhibited potent toxicity in neuronal and non-neuronal contexts; 2) nuclear localization was necessary and sufficient for this toxicity; 3) PR and GR toxicity was age-dependent and PR, but not GR, toxicity was influenced by mutations that uncouple physiological ageing from chronological ageing. Given that the toxicities of other ALS disease proteins are similarly modified by these mutations, our findings suggest that PR and other forms of ALS may share common disease mechanisms.

Results

Arginine-rich dipeptides are toxic in *C. elegans* motor neurons and muscle

Unconventional translation of the C9orf72-associated G₄C₂ repeats can produce several types of **d**i**p**eptide **r**epeat proteins (DPRs) (14). The nematode *C. elegans* contains a C9orf72 homolog, *alfa-1*, which is involved in ageing and stress responses, as well as stress-induced neurodegeneration (15). However, *alfa-1* does not contain G₄C₂ repeats and therefore does not model either RNA toxicity or RAN translation-induced DPR toxicity. To develop a *C. elegans* model for DPR expression, we generated constructs that express 50 repeats of four DPRs (GA, PA, GR, and PR). Each of these constructs utilizes codon-optimized sequences that encode for one dipeptide but eliminates the G₄C₂ repetitive sequence. Thus, our worm system is a ‘pure’ dipeptide model and does not contain repetitive GGGGCC sequences. To facilitate biochemical and cell biological detection of the DPRs, we inserted an in frame N-terminal FLAG epitope and a C-terminal green fluorescent protein (GFP) (Fig. 1A). Since ALS is a motor neuron disease, we used the motor neuron specific *unc-47* promoter to control expression and generated transgenic animals expressing each individual DPR.

Consistent with previous studies in yeast, *Drosophila*, and mammalian cells (5-8), we found that the arginine-rich DPRs were highly toxic in *C. elegans*. Animals expressing arginine-rich DPRs were viable, consistent with previous studies showing that *unc-47*+ motor neurons are not required for viability in *C. elegans* (16). However, motor neuron expressed (PR)₅₀ and (GR)₅₀ each led to significant reductions in motility (Fig. 1B). Motor neurons expressing (PR)₅₀ exhibited morphological signs of degeneration commonly observed in other *C. elegans* models of neurodegenerative diseases (17-19),

including commissure degeneration and membrane blebbing that were not observed in control animals or in animals expressing either (PA)₅₀ or (GA)₅₀ (Fig. 1C,D). These data show that arginine-containing dipeptides cause motility defects and neurodegenerative morphological changes when expressed in *C. elegans* motor neurons.

C. elegans motor neurons are extremely small (2-3 microns in diameter), making cell biological analysis of DPR localization in these cells difficult. Additionally, *C. elegans* neurons are highly resistant to RNA-interference mediated gene knockdown, which is commonly used to explore mechanisms of protein toxicity in *C. elegans* disease models (20, 21). To overcome these limitations, we expressed the DPRs in the larger muscle cells, which regulate motility and are a common site of expression for other *C. elegans* disease models (22-24). As we observed in motor neurons, muscle expression of arginine-rich dipeptides was highly toxic. Expression of either (PR)₅₀ or (GR)₅₀ in muscle led to completely penetrant embryonic and larval lethality that could be suppressed by feeding animals *gfp(RNAi)*-expressing bacteria (Fig. 2A, Table S1). *gfp(RNAi)*-sensitive embryonic or larval lethality was not observed in animals expressing either (PA)₅₀ or (GA)₅₀. (PR)₅₀ or (GR)₅₀ animals that were removed from *gfp(RNAi)* after embryonic development survived and went on to develop into adults. However, these DPR expressing adults exhibited age-onset paralysis. (Fig. 2B). (PR)₅₀ animals showed a significantly reduced lifespan which was not observed in (GR)₅₀ expressing animals (Fig. S1). The enhanced paralysis observed in (PR)₅₀ and (GR)₅₀ animals was not due to higher mRNA expression, since qPCR showed that all DPRs were expressed at similar levels (Fig. S2, Table S2). It was also not due to higher protein levels since *in vivo* imaging and flow cytometry quantification showed that (PR)₅₀-GFP and (GR)₅₀-GFP

fluorescence levels were significantly below those of all other DPRs (Fig. S3). The toxicity phenotype required protein production and was not due to any potential RNA effects, since (PR)₅₀ transgenic animals lacking a start ATG exhibited no detectable toxicity (Fig. S4). (PR)₅₀ toxicity was dependent on the number of repeats, as animals expressing 5, 15, or 25 repeats did not exhibit embryonic lethality (number of viable transgenic progeny (>L4) after 72 hours - (PR)₅-GFP – 139/145; (PR)₁₅-GFP – 68/75; (PR)₂₅-GFP – 114/117; p>0.1, Fisher's exact test). Adults expressing (PR)₅-GFP exhibited robust expression that appeared concentrated within almost all nuclei (Fig. 2C). Adults expressing both (PR)₁₅-GFP and (PR)₂₅-GFP expressed much lower levels of GFP as compared to (PR)₅-GFP, although the protein that was present also appeared to be concentrated within the nucleus and nucleolus (Fig. 2 C,D). Adults expressing (PR)₂₅ and (PR)₅₀, but not those expressing (PR)₅ or (PR)₁₅, exhibited accelerated age-onset paralysis (Fig. 2E), despite the fact that (PR)₂₅ was present at dramatically lower levels than (PR)₅, (Fig. 2D). Together, these studies show that arginine containing dipeptides exhibit developmental and post-developmental, age-dependent toxicity in *C. elegans* and in the case of the PR dipeptide, this toxicity is repeat-length dependent.

Toxic (GR)₅₀ and (PR)₅₀ dipeptides are localized to the nucleus and are not aggregated

To gain insight into the cell biological properties of (PR)₅₀ and (GR)₅₀ proteins, we examined their subcellular localization patterns in live animals expressing each DPR in the muscle. Animals expressing both GFP and non-toxic (PA)₅₀-GFP exhibited diffuse nuclear and non-nuclear GFP expression that was always excluded from the histone-free

nucleolar region (Fig. 3A,B). Muscle expressed (GA)₅₀-GFP formed intense non-nuclear puncta. In some cases, we noted (GA)₅₀-GFP signal in the nucleus but this nuclear localization was always diffuse and never in puncta (Fig. 3A,B). (GA)₅₀ non-nuclear exhibited little fluorescence recovery after photobleaching (FRAP; Fig. 4A,B), suggesting these puncta are highly immobilized protein aggregates. Muscle expressed (GR)₅₀-GFP and (PR)₅₀-GFP both exhibited substantially lower GFP levels than either of the other DPRs, despite their similar mRNA expression levels (Fig. S3), and appeared to be predominantly localized to the histone-free nucleolar region of the nucleus (Fig. 3A,B). Non-nuclear localization was always observed in (GR)₅₀ animals but was never observed in (PR)₅₀ animals (Fig. 3 A,B). Unlike what we observed for (GA)₅₀, FRAP analysis revealed that the nucleolar accumulations of (GR)₅₀ and (PR)₅₀ exhibited substantial fluorescence recovery after photobleaching that was significantly different from that of (GA)₅₀ (Fig. 4). The significant mobility of both (PR)₅₀ and (GR)₅₀ nuclear foci is inconsistent with the known biophysical properties of bona fide aggregates (25). Since both (PR)₅₀ and (GR)₅₀ appeared to be localized to the nucleolus, we compared their FRAP dynamics to those of FIB-1, which is homologous to the mammalian nucleolar protein fibrillarin (26). FIB-1 exhibited recovery kinetics that were similar to those of (GR)₅₀ and (PR)₅₀, suggesting that the dynamics of these two DPRs behave similarly to a bona fide nucleolar protein (Fig. 4C).

Nuclear localization is required for (PR)₅₀ and (GR)₅₀ toxicity

Given that toxic (PR)₅₀ and (GR)₅₀ in muscle were primarily localized to the nucleus, we asked if nuclear localization was necessary for their toxicity. To test this, we tethered each of the arginine-containing DPRs to a signal sequence-transmembrane domain (SS-TM) tag that restricts the DPR to cellular membranes with the DPR oriented on the cytosolic side of the membrane. In this context, the membrane-localized (PR)₅₀ and (GR)₅₀ were excluded from the nucleus (Fig. 5A). In contrast to soluble (PR)₅₀ and (GR)₅₀, membrane-localized (PR)₅₀ and (GR)₅₀ were viable in the absence of *gfp(RNAi)* and showed no age-dependent paralysis (Fig. 5B). We further tested whether nuclear localization was sufficient for toxicity by fusing the (PR)₅₀ DPR to the coding sequence for the *his-58* gene, which encodes a DNA binding histone only found in the nucleus. GFP-*his-58* expressing animals were viable and motile and exhibited strong nuclear GFP expression (Fig. 5 C,D). However, GFP-*his-58*-(PR)₅₀ expressing animals were not viable unless they were cultured under *gfp(RNAi)* conditions (number of viable transgenic progeny (>L4) / total progeny in the absence of GFP after 72 hours – GFP-*his-58* – 348/406; GFP-*his-58*-(PR)₅₀ - 9/56; p<0.0001, Fisher's exact test). Upon removal from *gfp(RNAi)*, *his-58*-(PR)₅₀ animals exhibited age-dependent paralysis (Fig. 5D) and this paralysis occurred with more rapid onset than in (PR)₅₀ animals (Fig. 5E), suggesting that nuclear localization further enhances (PR)₅₀ toxicity. The enhanced *his-58*-(PR)₅₀ toxicity was not due to higher expression levels of the transgene since GFP fluorescence levels of *his-58*-(PR)₅₀ was not higher than (PR)₅₀ (Fig. S5). Overall, these data show that nuclear localization is necessary and sufficient for (PR)₅₀ toxicity in *C. elegans*.

Post-mitotic age-dependent toxicity of (PR)₅₀ requires continuous dipeptide expression

Nuclear (PR)₅₀ exhibits age-dependent toxicity in *C. elegans*. This could be because (PR)₅₀ requires time to accumulate to sufficiently high levels necessary for toxicity. Alternatively, it could be because the cellular environment in aged animals is more permissive for toxicity. To test these models, we generated animals expressing DPR-GFP under the control of a heat shock inducible promoter (*hsp-16.2*). Following a brief (30 minutes) heat shock, we observed robust GFP expression of all DPRs in young adult animals. In most cases, the subcellular expression patterns for each DPR matched what we had observed previously, although the proteins were expressed more broadly across tissues due to the global activity of the heat shock promoter (Fig. 6A). Induction of (PR)₅₀ during embryonic development caused significant toxicity that was not observed in the absence of induction (Fig. 6B). Animals that had been induced to express (PR)₅₀ on day 1 of adulthood continued to exhibit normal motility and survival across their lifespan (Fig. 6C). However, continual daily induction of (PR)₅₀ protein eventually led to increased paralysis and death that was not observed in the control animals or in other DPR expressing animals, including those expressing (GR)₅₀. A single induction of (PR)₅₀ expression later in life (day 4 of adulthood) also failed to elicit any detectable phenotypes. The toxicity of (PR)₅₀ was not due to higher induction levels than other DPRs (Fig. S6). Therefore, the age-onset phenotypes of nuclear (PR)₅₀ in post-mitotic adult *C. elegans* require both continuous expression throughout life and an aged cellular environment.

Mutations that alter the rate of physiological ageing delay (PR)₅₀ age-dependent toxicity

The toxicity of (PR)₅₀ in an aged cellular environment could be due to the stochastic accumulation of toxic proteins levels or conformations over long periods of time. Alternatively, the process of ageing could lead to a decline in cellular processes that oppose (PR)₅₀ toxicity. To differentiate between these two hypotheses, we tested the role of the ageing process in the toxicity of (PR)₅₀. If (PR)₅₀ toxicity is due to accumulation of toxic protein levels/conformation over time, lifespan-extending conditions should have no effect on the rate of toxicity. However, if the ageing process actively regulates (PR)₅₀ toxicity, alterations in the rate of ageing should enhance (lifespan shortening) or suppress (lifespan extending) the toxicity of (PR)₅₀. The insulin signaling pathway is the most well characterized pathway that regulates lifespan and youthfulness from worms to humans (27). Mutations in this pathway are thought to extend lifespan by promoting a youthful cellular physiological state and therefore separate chronological and physiological states of ageing. In *C. elegans*, the *daf-2* gene encodes the homolog of the insulin/IGF receptor. Loss of function mutations in *daf-2* exert their effects via signaling-dependent activation of the FOXO transcription factor *daf-16*, as well as the heat shock transcription factor *hsf-1* (28). Mutations in *daf-16* and *hsf-1* suppress phenotypes associated with *daf-2* mutations and accelerate the rate of ageing (27).

To determine whether the toxicity of (PR)₅₀ is stochastic or enabled by declining physiological processes, we crossed the (PR)₅₀ transgene into the *daf-2(e1370);daf-16(mu86)* and segregated all possible (PR)₅₀ genotypes. If (PR)₅₀ toxicity is stochastic, then reduced insulin signaling should not alter the age-related phenotypes. However, if (PR)₅₀ toxicity is due to declining cellular physiology, then alterations in the rate of

ageing should slow the initiation and progression of toxicity. We found that in the *daf-2* mutant background, age-dependent declines in (PR)₅₀ motility were significantly reduced (Fig. 7A). These *daf-2* dependent phenotypes were suppressed in a *daf-2; daf-16* double mutant and were accelerated in the *daf-16* mutant background (Fig. 7B). Likewise, a mutation in the heat shock transcription factor *hsf-1*, which accelerates the rate of ageing (29), enhanced the toxicity of (PR)₅₀ (Fig. 7C). Interestingly, the protective effects of the *daf-2* mutant were not observed in (GR)₅₀ expressing animals (Fig. 7A). The protective effects of insulin signaling appear to act downstream from DPR accumulation and nuclear localization, as DPR abundance and subcellular distribution did not appear to be altered in any of these genetic backgrounds (Fig. 7D, E, F). We also found that in motor neurons expressing (PR)₅₀, *daf-2* reduced the levels of neurodegeneration-associated membrane blebbing (Figure S7). These data demonstrate that alterations in the rate of ageing impact (PR)₅₀ toxicity in both *C. elegans* muscle cells and motor neurons and suggest that (PR)₅₀ toxicity is not stochastic but is dependent on the cellular ageing process. Additionally, they suggest that (PR)₅₀ and (GR)₅₀ are toxic through partially distinct mechanisms since enhanced DAF-16/FOXO activation protects (PR)₅₀ animals but has no protective effects on (GR)₅₀ animals.

Discussion

In this study, we developed the first *C. elegans* model for C9orf72 dipeptide toxicity. We discovered that 1) (PR)₅₀ and (GR)₅₀ dipeptides are toxic in neuronal and non-neuronal contexts 2) both toxic dipeptides exhibit a shared nucleolar localization 3) nuclear localization of both (PR)₅₀ and (GR)₅₀ dipeptides is required for toxicity 4) post-mitotic toxicity of (PR)₅₀ is age-dependent 5) age-dependent toxicity of (PR)₅₀ is modified by genetic pathways that accelerate or decelerate the rate of physiological ageing in both muscle and motor neurons while (GR)₅₀ toxicity is not modified by these pathways. While some of these findings (i.e. points 1 and 2) are consistent with recent studies from yeast, *Drosophila*, and mammalian cells, others leverage the unique strengths of *C. elegans* to examine questions that either have not or cannot be addressed in other systems (i.e. points 3, 4, and 5). While many of our findings are consistent with studies using other C9 animal models, there are also significant differences. For example, a recent report describes toxicity associated with (GA) dipeptides in zebrafish (30). However, we find no evidence of (GA) toxicity in *C. elegans* when expressed in either motor neurons or muscle or more globally after heat shock, even though (GA) aggregates are observed in all of these conditions. The lack of toxicity of GA in worms compared to fish could be due to differences in repeat number (50 in worms vs. 80 in fish) or differences in expression levels. In another example, we found prominent nucleolar (GR)₅₀ localization, whereas a recent post-mortem study of C9orf72 carrier brains revealed perinuclear GR aggregates (31). Such discrepancies could reflect differences in dipeptide repeat length (50 repeats in our model vs. unknown repeats in patient cells) or in live animal vs post mortem sample fixation and preparation. Overall,

our findings suggest that this new *C. elegans* model, in conjunction with high throughput genetic and pharmacological screening methods, will be a useful and complementary system for exploring the mechanisms underlying C9orf72-associated DPR toxicity.

Results from our work suggest that the localization of (PR) and (GR) dipeptides to the nucleus is essential for their toxicity. This is consistent with several recent studies that suggest both PR and GR DPRs exert their toxicity by interfering with nuclear functions and nuclear pores (8, 12, 13, 32, 33). For example, in yeast, overexpression of nuclear import pathways, ribosome biogenesis pathways, and nuclear RNA binding proteins strongly modify (PR)₅₀ toxicity (8). Likewise, knockdown of *Drosophila* genes implicated in nuclear transport also modify PR toxicity (34). In most systems, including our new *C. elegans* model, both (PR)₅₀ and (GR)₅₀ DPRs exhibit prominent nucleolar localization. However, notable non-nuclear localization is also observed, especially in the case of the (GR)₅₀ dipeptide. Our FRAP data suggests that while (GA)₅₀ dipeptides are clearly protein aggregates, nuclear (PR)₅₀ and (GR)₅₀ are not protein aggregates, since, unlike (GA)₅₀, they exhibit significant recovery upon photobleaching. This localization pattern, as well as the pattern of genetic modifiers identified from yeast and *Drosophila* screens, has led to the hypothesis that (PR)₅₀ and (GR)₅₀ toxicity may occur through direct interactions within the nucleus. Alternatively, (PR)₅₀ and (GR)₅₀ could cause toxicity via non-nuclear interactions that then impinge on nuclear functions. Findings from our *C. elegans* model strongly support the former hypothesis, since we found that preventing nuclear localization completely abrogated the toxicity of the arginine-containing DPRs. We also found that forcing (PR)₅₀ into the nucleus maintained, and perhaps enhanced, toxicity. Our findings do not preclude the additional possibility

that freely soluble cytoplasmic DPRs could also mediate toxicity, since our method of preventing nuclear accumulation restricted DPRs to cytosolic membranes, which would also remove freely soluble cytoplasmic DPRs. Moreover, our method for restricting DPRs to the nucleus could result in unusual toxicity mediated by charge interactions between positively charged DPRs and negatively charged DNA. Unfortunately, attempts at using traditional NLS/NES sequence to drive DPRs into or out of the nucleus were unsuccessful for unknown reasons. Nevertheless, our findings are consistent with recent work showing that these DPRs specifically interact with low-complexity nuclear and nucleolar proteins that shape the formation of non-membrane bound organelles within the nucleus (12).

Worms have been utilized to model other genetic forms of ALS, including those associated with mutant forms of proteins such as superoxide dismutase 1 (SOD1) (17, 23, 35-38), TAR DNA binding protein 43 (TDP-43) (39-43), and fused in sarcoma (FUS) (39). In each of these cases, the worm model expresses a mutant protein that forms protein aggregates. The toxicity associated with the SOD1 and TDP-43 models is responsive to the activation state of the *daf-2*/insulin signaling pathway (41, 44). One of the major mechanisms by which the *daf-2*/insulin signaling pathway is thought to oppose these proteotoxic disease models is via the upregulation of genes that maintain protein folding (i.e. chaperones) or enhance the clearance of misfolded/aggregated proteins (i.e. proteases)(21). The overall effect of these targets is to delay the proteotoxic consequences of ageing, thus making mutants in the *daf-2*/insulin pathway tools for separating physiological ageing from chronological ageing. Like SOD1 and TDP-43, we found that (PR)₅₀ can also be suppressed by activating insulin signaling. However, unlike

SOD1 and TDP-43, (PR)₅₀ did not form detectable protein aggregates. Given that mutations in genes comprising the *daf-2*/insulin signaling pathway can modify all three disease models, this suggests that (PR)₅₀ may share common toxicity mechanisms with SOD1 and TDP-43, for example via disruptions in protein homeostasis. Interestingly, insulin signaling did not appear to alter DPR abundance or subcellular localization in our model, suggesting that this pathway may act downstream from DPR nuclear functions to provide toxicity protection. Future genetic modifier screens should reveal the identity of such mechanisms, as well as whether DPRs and other ALS disease genes share common disease mechanisms. The powerful phenotypes elicited by (PR)₅₀ in our *C. elegans* model, as well as the tractability of genome-wide RNAi approaches, will facilitate such screens.

Despite the fact that both (PR)₅₀ and (GR)₅₀ are required in the nucleus to exert their toxicity, we found important differences between their mechanisms of toxicity. For example, the toxicity associated with (PR)₅₀ was sensitive to manipulations in the activation state of the *daf-2*/insulin signaling pathway. In the *daf-2* mutant background, (PR)₅₀ toxicity was delayed, whereas in the *daf-16* and *hsf-1* mutant background, (PR)₅₀ toxicity was enhanced. Curiously, (PR)₅₀ toxicity in the *daf-2;daf-16* background was suppressed, although not to the levels seen with *daf-16* alone. This could be due to variability in assay conditions. Alternatively, it could suggest that *daf-2* engages other factors, such as *skn-1* (45) and/or *hsf-1* (28, 46), in addition to *daf-16* to mediate protection against (PR)₅₀ toxicity. However, (GR)₅₀ toxicity was unaffected by the *daf-2*/insulin pathway activation state. Additionally, acute induction of (PR)₅₀ using a heat shock-inducible promoter led to toxicity, while acute induction of (GR)₅₀ did not produce

toxicity. These observations suggests that (PR)₅₀ and (GR)₅₀ exert different types of toxicity and that only (PR)₅₀ toxicity is susceptible to the consequences of *daf-2*/insulin pathway activation. The ability of insulin/IGF signaling to modify toxicity of one dipeptide but not another may partially explain the failure of insulin/IGF therapies in ALS clinical trials among patients with C9orf72 mutations (47-49). Perhaps additional therapies targeting insulin/IGF independent toxicity like that associated with (GR)₅₀ could be used in combinatorial therapies to protect against the multiple forms of toxicity associated with C9orf72 mutations. Comparative genetic modifier screens, as well as comparative RNAseq studies, should be useful in determining how cells differentially respond to these two DPRs.

RAN translation products are an emerging component of several nucleotide repeat expansion disorders, including C9orf72-associated FTD/ALS and CAG-associated Huntington's disease (50). *C. elegans* is a particularly attractive model for identifying the mechanisms underlying the toxicity of these various RAN proteins. Given the strong phenotypes described here for the C9orf72-associated (PR)₅₀ and (GR)₅₀ RAN products, genetic and pharmacological screens should prove to be a valuable approach for identifying the genes and pathways that are required for these and perhaps other RAN protein-mediated toxicity. In addition to delineating mechanisms of DPR toxicity, *C. elegans* may also prove useful in defining the requirements for RAN translation. Worms expressing pure GGGGCC repeats were recently described (51, 52). These studies suggest that G₄C₂ repeat expression produces RNA foci, dipeptide protein expression, and toxicity in the form of a shortened lifespan and paralysis, although whether such toxicity was due to the expression of dipeptides was not determined. If such RAN

products were tagged with GFP and these RAN-GFP products were easily detectable, high-throughput genetic approaches could be used to decipher the genetic, cellular, and age-dependent requirements for RAN translation *in vivo*.

In conclusion, we developed the first *C. elegans* model for C9orf72-associated dipeptide repeat protein toxicity. Our findings reveal prominent roles for protein localization and ageing in the toxicity of arginine-containing dipeptides and suggest significant differences in the response of the DPRs to protective genetic pathways. Using these phenotypes, our future studies will utilize the genetic and pharmacological accessibility of worms to better define the mechanisms of dipeptide repeat protein toxicity. Given the conserved nature of worm genetics, we anticipate that our findings may guide new ideas for treatments or biomarkers in C9orf72 associated diseases.

Materials and methods

C. elegans strains and culture

Strains were cultured on standard NGM media with *E.coli* OP50 bacteria. Strains expressing (PR)₅₀ and (GR)₅₀ DPRs were cultured on *gfp(RNAi)* bacteria at 20°C until the experiment, when they were shifted to OP50. The following strains were used; *daf-2(e1370)*, *daf-16(mu86)*, *hsf-1(sy441)*. Standard genetic approaches were utilized to cross mutants into the DPR backgrounds. The homozygous genotype of every strain was confirmed by DNA sequencing of the mutant lesion. Wild type animals were re-isolated in every cross and utilized as the DPR only control in resulting experiments. DPR toxicity studies were carried out using animals grown at 25°C, unless otherwise noted.

Molecular Biology and Transgenics

Codon-varied dipeptide sequences were isolated from previously described plasmids (6) (nucleotide sequences can be found in Table S3). (PR)₅, (PR)₁₅, and (PR)₂₅ codon-varied plasmids were synthesized (GeneArt, ThermoFisher Scientific, Waltham, MA). Dipeptide sequences were isolated as a *HindIII* / *BamHI* fragment and subcloned into the *C. elegans* expression vector pPD95.79 to generate dipeptide with a C-terminal GFP tag. Promoters were PCR amplified, incorporating both a 3XFLAG epitope immediately downstream from the start ATG and *HindIII* sites flanking the fragment. Promoters were subcloned into the DPR-pPD95.79 vectors as *HindIII* fragments. To make N-terminal GFP-(PR)₅₀ and GFP-(GR)₅₀ fusions, GFP was PCR amplified and cloned in frame with the start codon of the *myo-3* promoter. The dipeptide sequences were subcloned as a

HindIII / *BamHI* fragment into the pPD49.26 expression vector. The *myo-3-GFP* fragment was then subcloned into the DPR-pPD49.26 as a *HindIII* fragment. The membrane-bound DPRs were generated by a PCR fusion method. We first amplified the signal sequence and transmembrane domain from the *pat-3* gene as supplied in vector pPD122.39. The membrane domain was then fused to the *myo-3* promoter in-frame with the start ATG and then subcloned as a *HindIII* fragment into the DPR-pPD95.79 vectors. The resulting clones produce a membrane-localized DPR with the DPR facing the cytoplasm. To make the *his-58*-DPR fusions, the *his-58* genomic sequence was PCR amplified and Gibson cloned (New England Biolabs, Ipswich, MA) into the *myo-3p::GFP* sequence downstream of and in-frame with the GFP sequence. The resulting *myo-3p::GFP-his-58* fragment was subcloned as a *HindIII* fragment into the DPR-pPD49.26 vectors. Primer sequences and plasmids utilized for this study are available upon request. A list of nucleotide sequences for promoters used in this study can be found in Table S4.

Transgenic worms were generated by injecting the DPR construct (20ng/μl) and the *myo-3p::mCherry* pCFJ104 or *myo-3p::dsRed2* marker plasmid (100ng/μl) into the gonad of wild type animals. Transgenes were integrated using a standard gamma-ray (Cs^{137}) mutagenesis, followed by selection of animals exhibiting 100% transmission of the mCherry marker. Integrated strains were outcrossed six times to wild type animals. In the case of (PR)₅₀ and (GR)₅₀, injected animals were maintained on *gfp(RNAi)* plates until the experimental assay was performed. All procedures involving recombinant or synthetic nucleic acid molecules and materials were approved by the University of Pittsburgh Institutional Biosafety Committee.

Microscopy

Worms were anesthetized (10mM levamisole) and mounted on agar pads for fluorescence microscopy. Images were collected on either a Leica MZ16FA stereo dissecting scope or a Leica DMI4000 inverted microscope and a Leica DFC 340Fx digital camera (Leica Microsystems, Wetzlar, Germany). Z-stack images were deconvolved using Leica AF6000 software. Unless noted, images within an experiment were collected using the same exposure settings and processed with identical deconvolution parameters.

FRAP studies were carried out on levamisole anesthetized day 1 adult hermaphrodites using a Leica DMI8 confocal microscope at the University of Pittsburgh Center for Biologic Imaging. Images were captured at 20-30 Hz. Following imaging of baseline fluorescence, a region of interest corresponding to a portion of the nuclear or cytoplasmic foci was photobleached and fluorescence recovery within the photobleached area was monitored over at least 60 seconds. Data were normalized so that the image preceding the photobleach was set to 100 percent and the first image following the photobleach was set to zero percent. Imaging conditions over the time course of the experiment caused minimal loss of signal, suggesting an absence of photobleaching during the monitoring period. Photobleaching of the entire foci led to no recovery of signal over the imaging time period, suggesting that any resulting new signal was due to diffusion of molecules within the foci rather than exchange of new molecules outside of the foci.

To quantify DPR subcellular localization of the DPRs, we co-expressed each DPR with a *myo-3p::tagRFP-his-58* transgene to mark the nucleus. Z-stack images were collected for 1-21 nuclei across 5-6 individual animals, looking at at least 55 nuclei per DPR. We scored each nucleus for DPR expression in the histone-free region of the nucleus ('Nucleolar'), histone positive region of the nucleus ('Nuclear'), and outside of the histone marker ('Non-nuclear'). The percentage of each category in each worm was determined and used to calculate and mean \pm S.D. for each category.

Paralysis and thrashing assays

For all assays except for that shown in Figures 5D and 5E, gravid DPR expressing transgenic animals were moved from *gfp(RNAi)* to OP50 plates and allowed to lay eggs for 24 hours. The resulting progeny were allowed to grow up on OP50, permitting DPR accumulation. Ten L4 animals were placed on each of 3-5 plates (N=30-50 per assay). Each day, animals that failed to move at least half a body length in response to manual stimulation with a platinum wire but were still alive (pharyngeal pumping, movement of less than half a body length) were scored as paralyzed. Animals that died, desiccated on the plate edges, or exhibited internal hatching of progeny were censored from the assay. Each day, mobile animals were transferred to a new plate and paralyzed, dead, and censored animals were removed from the assay. For the assay in Figures 5D and 5E, *his-58-(PR)₅₀* progeny from animals moved from *gfp(RNAi)* to OP50 were not viable, presumably due to the enhanced toxicity of the nuclear localized (PR)₅₀ protein. Therefore, for these assays, animals were removed from *gfp(RNAi)* as L4 stage animals,

placed on OP50 at 25°C, and motility in the animals moved from *gfp(RNA)* was monitored as described above. Since animals are removed from the assay once they are scored as paralyzed, it is not appropriate to utilize statistical approaches that compare means and errors between time points (i.e. T-tests, ANOVA tests). Instead, we utilized the Log-rank statistical method, a cumulative statistical approach that compares changes in population sizes over time for a specified endpoint (53). Because this end-point assay is cumulative and not replicative, data points do not contain error bars. For each assay, 2-3 independent trials with 45-50 animals per assay were performed and the results from one representative trial are shown.

To measure thrashing, animals were maintained at 25°C on OP50, and transgenic animals for each strain were picked as L4's the day before the experiment. The following day, worms were placed on clean NGM plates and allowed to move freely for 10 minutes so that most of the bacteria came off the animal before the experiment. Worms were then placed individually into 3cm petri dishes containing M9 buffer and allowed to adjust to the new environment for 5 minutes. The worms were then observed for 30 seconds and the number of thrashes (reversal of body bend that crosses the midline) was counted. We were unable to score thrashing in *daf-2(e1370)* animals since this mutation on its own causes significant defects in liquid thrashing.

Brood size assays

For brood size assays, at least 10 L4 stage animals were individually picked to OP50-containing NGM plates at 25 degrees and transferred to a new plate every 24 hours

until cessation of egg laying. Each plate was allowed to age for 48-72 hours and the number of animals \geq L4 stage of development was counted. Brood sizes were normalized within each strain to the mean brood size of animals grown on *gfp(RNAi)* bacteria.

Neurodegeneration assays

L4 animals of the indicated genotype were isolated at 25°C and imaged 24 hours later as ‘Day 1 adults’. All of the strains contained an *unc-47p::GFP* marker to reveal GABA motor neuron morphology. Animals were anesthetized in levamisole and Z-series images of GABAergic commissures were collected. Commissure breaks were identified as interruptions in the GFP signal surrounded by dorsal and ventral GFP in the commissures. Blebbing was scored only in the commissures and was identified by the presence of one or more GFP varicosities. For assays involving *daf-2*, we were unable to score either membrane blebbing or commissure breakage in (GR)₅₀ expressing animals because the neuronal GFP marker used to score such events was undetectable, likely due to significant neurodegeneration that continued to occur in (GR)₅₀; *daf-2* animals.

Statistical Analysis

Paralysis assays were analyzed using the Kaplan-Meier log-rank function (OASIS (54, 55)). Comparisons of means were analyzed with either a two-tailed Students t-test (2

groups) or ANOVA (3 or more groups) using the Tukey or Dunn's post-test analysis as indicated in GraphPad Prism 7 (GraphPad Software, Inc., La Jolla, CA). p-values of <0.05 were considered significant.

Acknowledgements

This work was supported by grants from the NIH (NS094921 (U.P. and T.L.), 1S10OD021540 (S.C.W) and NS096319 (T.L.)) and the Israeli Binational Science Foundation Grant (2011323 (T.L.)). Some strains were provided by the CGC, which is funded by NIH Office of Research Infrastructure Programs (P40 OD010440).

Conflict of Interest Statement

The authors have no conflicts of interests to declare

References

- 1 DeJesus-Hernandez, M., Mackenzie, I.R., Boeve, B.F., Boxer, A.L., Baker, M., Rutherford, N.J., Nicholson, A.M., Finch, N.A., Flynn, H., Adamson, J. *et al.* (2011) Expanded GGGGCC hexanucleotide repeat in noncoding region of C9ORF72 causes chromosome 9p-linked FTD and ALS. *Neuron*, **72**, 245-256.
- 2 Renton, A.E., Majounie, E., Waite, A., Simon-Sanchez, J., Rollinson, S., Gibbs, J.R., Schymick, J.C., Laaksovirta, H., van Swieten, J.C., Myllykangas, L. *et al.* (2011) A hexanucleotide repeat expansion in C9ORF72 is the cause of chromosome 9p21-linked ALS-FTD. *Neuron*, **72**, 257-268.
- 3 Ling, S.C., Polymenidou, M. and Cleveland, D.W. (2013) Converging mechanisms in ALS and FTD: disrupted RNA and protein homeostasis. *Neuron*, **79**, 416-438.
- 4 Su, Z., Zhang, Y., Gendron, T.F., Bauer, P.O., Chew, J., Yang, W.Y., Fostvedt, E., Jansen-West, K., Belzil, V.V., Desaro, P. *et al.* (2014) Discovery of a biomarker and lead small molecules to target r(GGGGCC)-associated defects in c9FTD/ALS. *Neuron*, **83**, 1043-1050.
- 5 Mizielinska, S., Gronke, S., Niccoli, T., Ridler, C.E., Clayton, E.L., Devoy, A., Moens, T., Norona, F.E., Woollacott, I.O., Pietrzyk, J. *et al.* (2014) C9orf72 repeat expansions cause neurodegeneration in Drosophila through arginine-rich proteins. *Science*, **345**, 1192-1194.
- 6 Wen, X., Tan, W., Westergard, T., Krishnamurthy, K., Markandaiah, S.S., Shi, Y., Lin, S., Shneider, N.A., Monaghan, J., Pandey, U.B. *et al.* (2014) Antisense Proline-Arginine RAN Dipeptides Linked to C9ORF72-ALS/FTD Form Toxic Nuclear Aggregates that Initiate In Vitro and In Vivo Neuronal Death. *Neuron*, **84**, 1213-1225.
- 7 Kwon, I., Xiang, S., Kato, M., Wu, L., Theodoropoulos, P., Wang, T., Kim, J., Yun, J., Xie, Y. and McKnight, S.L. (2014) Poly-dipeptides encoded by the C9orf72 repeats bind nucleoli, impede RNA biogenesis, and kill cells. *Science*, **345**, 1139-1145.
- 8 Jovicic, A., Mertens, J., Boeynaems, S., Bogaert, E., Chai, N., Yamada, S.B., Paul, J.W., 3rd, Sun, S., Herdy, J.R., Bieri, G. *et al.* (2015) Modifiers of C9orf72 dipeptide repeat toxicity connect nucleocytoplasmic transport defects to FTD/ALS. *Nature neuroscience*, **18**, 1226-1229.
- 9 Davidson, Y.S., Barker, H., Robinson, A.C., Thompson, J.C., Harris, J., Troakes, C., Smith, B., Al-Saraj, S., Shaw, C., Rollinson, S. *et al.* (2014) Brain distribution of dipeptide repeat proteins in frontotemporal lobar degeneration and motor neurone disease associated with expansions in C9ORF72. *Acta neuropathologica communications*, **2**, 70.
- 10 Mackenzie, I.R., Arzberger, T., Kremmer, E., Troost, D., Lorenzl, S., Mori, K., Weng, S.M., Haass, C., Kretzschmar, H.A., Edbauer, D. *et al.* (2013) Dipeptide repeat protein pathology in C9ORF72 mutation cases: clinico-pathological correlations. *Acta neuropathologica*, **126**, 859-879.
- 11 Cleary, J.D. and Ranum, L.P. (2014) Repeat associated non-ATG (RAN) translation: new starts in microsatellite expansion disorders. *Current opinion in genetics & development*, **26**, 6-15.

- 12 Lee, K.H., Zhang, P., Kim, H.J., Mitrea, D.M., Sarkar, M., Freibaum, B.D., Cika, J., Coughlin, M., Messing, J., Molliex, A. *et al.* (2016) C9orf72 Dipeptide Repeats Impair the Assembly, Dynamics, and Function of Membrane-Less Organelles. *Cell*, **167**, 774-788 e717.
- 13 Lin, Y., Mori, E., Kato, M., Xiang, S., Wu, L., Kwon, I. and McKnight, S.L. (2016) Toxic PR Poly-Dipeptides Encoded by the C9orf72 Repeat Expansion Target LC Domain Polymers. *Cell*, **167**, 789-802 e712.
- 14 Zu, T., Liu, Y., Banez-Coronel, M., Reid, T., Pletnikova, O., Lewis, J., Miller, T.M., Harms, M.B., Falchook, A.E., Subramony, S.H. *et al.* (2013) RAN proteins and RNA foci from antisense transcripts in C9ORF72 ALS and frontotemporal dementia. *Proceedings of the National Academy of Sciences of the United States of America*, **110**, E4968-4977.
- 15 Therrien, M., Rouleau, G.A., Dion, P.A. and Parker, J.A. (2013) Deletion of C9ORF72 results in motor neuron degeneration and stress sensitivity in *C. elegans*. *PloS one*, **8**, e83450.
- 16 McIntire, S.L., Jorgensen, E. and Horvitz, H.R. (1993) Genes required for GABA function in *Caenorhabditis elegans*. *Nature*, **364**, 334-337.
- 17 Li, J., Huang, K.X. and Le, W.D. (2013) Establishing a novel *C. elegans* model to investigate the role of autophagy in amyotrophic lateral sclerosis. *Acta pharmacologica Sinica*, **34**, 644-650.
- 18 Aggad, D., Veriepe, J., Tauffenberger, A. and Parker, J.A. (2014) TDP-43 toxicity proceeds via calcium dysregulation and necrosis in aging *Caenorhabditis elegans* motor neurons. *The Journal of neuroscience : the official journal of the Society for Neuroscience*, **34**, 12093-12103.
- 19 Earls, L.R., Hacker, M.L., Watson, J.D. and Miller, D.M., 3rd. (2010) Coenzyme Q protects *Caenorhabditis elegans* GABA neurons from calcium-dependent degeneration. *Proceedings of the National Academy of Sciences of the United States of America*, **107**, 14460-14465.
- 20 Nollen, E.A., Garcia, S.M., van Haften, G., Kim, S., Chavez, A., Morimoto, R.I. and Plasterk, R.H. (2004) Genome-wide RNA interference screen identifies previously undescribed regulators of polyglutamine aggregation. *Proceedings of the National Academy of Sciences of the United States of America*, **101**, 6403-6408.
- 21 Cohen, E., Bieschke, J., Perciavalle, R.M., Kelly, J.W. and Dillin, A. (2006) Opposing activities protect against age-onset proteotoxicity. *Science*, **313**, 1604-1610.
- 22 Satyal, S.H., Schmidt, E., Kitagawa, K., Sondheimer, N., Lindquist, S., Kramer, J.M. and Morimoto, R.I. (2000) Polyglutamine aggregates alter protein folding homeostasis in *Caenorhabditis elegans*. *Proceedings of the National Academy of Sciences of the United States of America*, **97**, 5750-5755.
- 23 Gidalevitz, T., Krupinski, T., Garcia, S. and Morimoto, R.I. (2009) Destabilizing protein polymorphisms in the genetic background direct phenotypic expression of mutant SOD1 toxicity. *PLoS genetics*, **5**, e1000399.
- 24 Bank, E.M., Ben-Harush, K., Feinstein, N., Medalia, O. and Gruenbaum, Y. (2012) Structural and physiological phenotypes of disease-linked lamin mutations in *C. elegans*. *Journal of structural biology*, **177**, 106-112.
- 25 Brignull, H.R., Morley, J.F., Garcia, S.M. and Morimoto, R.I. (2006) Modeling polyglutamine pathogenesis in *C. elegans*. *Methods in enzymology*, **412**, 256-282.

- 26 Allen, A.K., Nesmith, J.E. and Golden, A. (2014) An RNAi-based suppressor screen identifies interactors of the Myt1 ortholog of *Caenorhabditis elegans*. *G3*, **4**, 2329-2343.
- 27 Murphy, C.T. and Hu, P.J. (2013) Insulin/insulin-like growth factor signaling in *C. elegans*. *WormBook : the online review of C. elegans biology*, in press., 1-43.
- 28 Hsu, A.L., Murphy, C.T. and Kenyon, C. (2003) Regulation of aging and age-related disease by DAF-16 and heat-shock factor. *Science*, **300**, 1142-1145.
- 29 Garigan, D., Hsu, A.L., Fraser, A.G., Kamath, R.S., Ahringer, J. and Kenyon, C. (2002) Genetic analysis of tissue aging in *Caenorhabditis elegans*: a role for heat-shock factor and bacterial proliferation. *Genetics*, **161**, 1101-1112.
- 30 Ohki, Y., Wenninger-Weinzierl, A., Hruscha, A., Asakawa, K., Kawakami, K., Haass, C., Edbauer, D. and Schmid, B. (2017) Glycine-alanine dipeptide repeat protein contributes to toxicity in a zebrafish model of C9orf72 associated neurodegeneration. *Molecular neurodegeneration*, **12**, 6.
- 31 Flores, B.N., Dulchavsky, M.E., Krans, A., Sawaya, M.R., Paulson, H.L., Todd, P.K., Barmada, S.J. and Ivanova, M.I. (2016) Distinct C9orf72-Associated Dipeptide Repeat Structures Correlate with Neuronal Toxicity. *PloS one*, **11**, e0165084.
- 32 Freibaum, B.D., Lu, Y., Lopez-Gonzalez, R., Kim, N.C., Almeida, S., Lee, K.H., Badders, N., Valentine, M., Miller, B.L., Wong, P.C. *et al.* (2015) GGGGCC repeat expansion in C9orf72 compromises nucleocytoplasmic transport. *Nature*, **525**, 129-133.
- 33 Zhang, K., Donnelly, C.J., Haeusler, A.R., Grima, J.C., Machamer, J.B., Steinwald, P., Daley, E.L., Miller, S.J., Cunningham, K.M., Vidensky, S. *et al.* (2015) The C9orf72 repeat expansion disrupts nucleocytoplasmic transport. *Nature*, **525**, 56-61.
- 34 Boeynaems, S., Bogaert, E., Michiels, E., Gijssels, I., Sieben, A., Jovicic, A., De Baets, G., Scheveneels, W., Steyaert, J., Cuijt, I. *et al.* (2016) *Drosophila* screen connects nuclear transport genes to DPR pathology in c9ALS/FTD. *Scientific reports*, **6**, 20877.
- 35 Li, J., Li, T., Zhang, X., Tang, Y., Yang, J. and Le, W. (2014) Human superoxide dismutase 1 overexpression in motor neurons of *Caenorhabditis elegans* causes axon guidance defect and neurodegeneration. *Neurobiology of aging*, **35**, 837-846.
- 36 Thompson, M.L., Chen, P., Yan, X., Kim, H., Borom, A.R., Roberts, N.B., Caldwell, K.A. and Caldwell, G.A. (2014) TorsinA rescues ER-associated stress and locomotive defects in *C. elegans* models of ALS. *Disease models & mechanisms*, **7**, 233-243.
- 37 Wang, J., Farr, G.W., Hall, D.H., Li, F., Furtak, K., Dreier, L. and Horwich, A.L. (2009) An ALS-linked mutant SOD1 produces a locomotor defect associated with aggregation and synaptic dysfunction when expressed in neurons of *Caenorhabditis elegans*. *PLoS genetics*, **5**, e1000350.
- 38 Oeda, T., Shimohama, S., Kitagawa, N., Kohno, R., Imura, T., Shibasaki, H. and Ishii, N. (2001) Oxidative stress causes abnormal accumulation of familial amyotrophic lateral sclerosis-related mutant SOD1 in transgenic *Caenorhabditis elegans*. *Human molecular genetics*, **10**, 2013-2023.
- 39 Vaccaro, A., Tauffenberger, A., Aggad, D., Rouleau, G., Drapeau, P. and Parker, J.A. (2012) Mutant TDP-43 and FUS cause age-dependent paralysis and neurodegeneration in *C. elegans*. *PloS one*, **7**, e31321.

- 40 Liachko, N.F., Guthrie, C.R. and Kraemer, B.C. (2010) Phosphorylation promotes neurotoxicity in a *Caenorhabditis elegans* model of TDP-43 proteinopathy. *The Journal of neuroscience : the official journal of the Society for Neuroscience*, **30**, 16208-16219.
- 41 Zhang, T., Mullane, P.C., Periz, G. and Wang, J. (2011) TDP-43 neurotoxicity and protein aggregation modulated by heat shock factor and insulin/IGF-1 signaling. *Human molecular genetics*, **20**, 1952-1965.
- 42 Ash, P.E., Zhang, Y.J., Roberts, C.M., Saldi, T., Hutter, H., Buratti, E., Petrucelli, L. and Link, C.D. (2010) Neurotoxic effects of TDP-43 overexpression in *C. elegans*. *Human molecular genetics*, **19**, 3206-3218.
- 43 Salazar, D.A., Butler, V.J., Argouarch, A.R., Hsu, T.Y., Mason, A., Nakamura, A., McCurdy, H., Cox, D., Ng, R., Pan, G. *et al.* (2015) The Progranulin Cleavage Products, Granulins, Exacerbate TDP-43 Toxicity and Increase TDP-43 Levels. *The Journal of neuroscience : the official journal of the Society for Neuroscience*, **35**, 9315-9328.
- 44 Boccitto, M., Lamitina, T. and Kalb, R.G. (2012) Daf-2 signaling modifies mutant SOD1 toxicity in *C. elegans*. *PloS one*, **7**, e33494.
- 45 Tullet, J.M., Hertweck, M., An, J.H., Baker, J., Hwang, J.Y., Liu, S., Oliveira, R.P., Baumeister, R. and Blackwell, T.K. (2008) Direct inhibition of the longevity-promoting factor SKN-1 by insulin-like signaling in *C. elegans*. *Cell*, **132**, 1025-1038.
- 46 Morley, J.F. and Morimoto, R.I. (2004) Regulation of longevity in *Caenorhabditis elegans* by heat shock factor and molecular chaperones. *Molecular biology of the cell*, **15**, 657-664.
- 47 Sacca, F., Quarantelli, M., Rinaldi, C., Tucci, T., Piro, R., Perrotta, G., Carotenuto, B., Marsili, A., Palma, V., De Michele, G. *et al.* (2012) A randomized controlled clinical trial of growth hormone in amyotrophic lateral sclerosis: clinical, neuroimaging, and hormonal results. *Journal of neurology*, **259**, 132-138.
- 48 Howe, C.L., Bergstrom, R.A. and Horazdovsky, B.F. (2009) Subcutaneous IGF-1 is not beneficial in 2-year ALS trial. *Neurology*, **73**, 1247; author reply 1247-1248.
- 49 Sorenson, E.J., Windbank, A.J., Mandrekar, J.N., Bamlet, W.R., Appel, S.H., Armon, C., Barkhaus, P.E., Bosch, P., Boylan, K., David, W.S. *et al.* (2008) Subcutaneous IGF-1 is not beneficial in 2-year ALS trial. *Neurology*, **71**, 1770-1775.
- 50 Banez-Coronel, M., Ayhan, F., Tarabochia, A.D., Zu, T., Perez, B.A., Tusi, S.K., Pletnikova, O., Borchelt, D.R., Ross, C.A., Margolis, R.L. *et al.* (2015) RAN Translation in Huntington Disease. *Neuron*, **88**, 667-677.
- 51 Kramer, N.J., Carlomagno, Y., Zhang, Y.J., Almeida, S., Cook, C.N., Gendron, T.F., Prudencio, M., Van Blitterswijk, M., Belzil, V., Couthouis, J. *et al.* (2016) Spt4 selectively regulates the expression of C9orf72 sense and antisense mutant transcripts. *Science*, **353**, 708-712.
- 52 Wang, X., Hao, L., Saur, T., Joyal, K., Zhao, Y., Zhai, D., Li, J., Pribadi, M., Coppola, G., Cohen, B.M. *et al.* (2016) Forward Genetic Screen in *Caenorhabditis elegans* Suggests F57A10.2 and *acp-4* As Suppressors of C9ORF72 Related Phenotypes. *Frontiers in molecular neuroscience*, **9**, 113.
- 53 Suci, G.P., Lemeshow, S. and Moeschberger, M. (2003) Balakrishnan, N. and Rao, C.R. (eds.), In *Handbook of Statistics*. Elsevier B.V., Vol. 23, pp. 251-262.

54 Han, S.K., Lee, D., Lee, H., Kim, D., Son, H.G., Yang, J.S., Lee, S.V. and Kim, S. (2016) OASIS 2: online application for survival analysis 2 with features for the analysis of maximal lifespan and healthspan in aging research. *Oncotarget*, in press.

55 Yang, J.S., Nam, H.J., Seo, M., Han, S.K., Choi, Y., Nam, H.G., Lee, S.J. and Kim, S. (2011) OASIS: online application for the survival analysis of lifespan assays performed in aging research. *PloS one*, **6**, e23525.

Figure legends

Figure 1 – Arginine-containing DPRs are toxic in motor neurons. (A) Molecular strategy for expression of codon-varied dipeptide repeat proteins in *C. elegans* (B) Liquid thrashing quantification of transgenic animals expressing the indicated DPR under the motor neuron-specific *unc-47* promoter. N=20 animals per genotype. Each symbol represents quantification for one animal, horizontal line indicates population median. *** - $p < 0.001$ vs GFP control, (One-way non-parametric ANOVA with Dunn's post-hoc test). (C) Representative images of *unc-47+* motor neurons in animals expressing the indicated DPR. Arrow points to an example of membrane blebbing. Arrowhead points to examples of commissure breaks. Scale bar = 10 microns (D) Quantification of membrane blebbing and commissure breaks in each of the indicated strains. For each animal, we counted the total number of commissures with blebbing or breaks and divided by the total number of detectable commissures. N=20 animals per genotype. Each symbol represents quantification for one animal expressed as a percentage. The horizontal line indicates population median with interquartile range. **** - $p < 0.0001$ vs GFP control (One-way non-parametric ANOVA with Dunn's post-hoc test). N=20 animals per genotype.

Figure 2 – Muscle expressed arginine-containing dipeptides are toxic in *C. elegans* (A) Brood size for worms expressing each integrated dipeptide protein in the presence or absence of *gfp(RNAi)* at 25°C. Data for each strain are normalized to the mean brood size of animals grown on *gfp(RNAi)*. *** - $p < 0.001$ (One-way ANOVA with post-hoc

Tukey test). Raw brood size data for 25°C are included in ‘Table S1’. (B) Paralysis assay for adult animals raised in the absence of *gfp(RNAi)*. N≥43-49 animals per genotype. *** - p<0.001 (Log-rank test with Bonferroni adjusted p-value), (C) Fluorescent microscopy of Day 1 adult hermaphrodites expressing (PR)₅-GFP, (PR)₁₅-GFP, (PR)₂₅-GFP, or (PR)₅₀-GFP (green) in the muscle. Muscle DNA (marked by a *myo-3p::his-58-mCherry* reporter) is in red. Arrows point to sites of nuclear GFP puncta. Scale bar = 10 microns. All images were acquired using identical exposure settings. The row labeled ‘*myo-3p::(PR)₅₀* (enhanced)’ was adjusted for brightness and contrast in the GFP channel differently from the other images so that the (PR)₅₀-GFP signal is observable. (D) Quantification of the GFP levels from the indicated PR repeat animals. Each point shows the measured value for a single nucleus, horizontal line indicates population median with interquartile range. ** - p<0.01, **** - p<0.0001 vs GFP control, (One-way non-parametric ANOVA with Dunn’s post-hoc test). (E) Paralysis assay of animals expressing the indicated number of (PR) repeats under the control of the *myo-3* promoter. ‘Day 0’ animals were isolated as L4 stage animals. N=48-50 animals per genotype. *** - p<0.001 vs. GFP control (Log-rank test with Bonferroni adjusted p-value).

Figure 3 – (PR)₅₀ and (GR)₅₀ are localized to the nucleolus in *C. elegans* muscle cells (A) Imaging of live, anesthetized day 1 adult *C. elegans* hermaphrodites expressing the indicated dipeptide. Green shows dipeptide-GFP localization expressed in muscle, red shows histone-tagRFP within the muscle nucleus. Arrowhead points to the histone-free nucleolar region. Scale bar – 10 microns. (B) Quantification of DPR-GFP signal that is

observed in nucleoplasm, nucleolus, and non-nuclear cellular compartments. N=55-78 nuclei from 5-6 animals. Data shown are means \pm S.D.

Figure 4 – Arginine-containing DPRs are not aggregates (A) Representative images from FRAP analysis of subcellular localized DPR proteins expressed in muscle. Dashed outline indicates site of photobleaching and post-bleaching quantification. Recovery images are 150 seconds post-bleach. Scale bar = 2 microns (B) Quantification of FRAP imaging. Data shown are mean \pm S.E.M. from 9-10 data sets per genotype. (C) Average equilibrium fluorescence recovery after 60 seconds. Data shown are mean \pm S.D. from 9-10 data sets per genotype. n.s. vs FIB-1-GFP (One-way ANOVA with Dunn's multiple comparison test).

Figure 5 – Nuclear localization of muscle expressed arginine-containing DPRs is necessary and sufficient for toxicity. (A) Representative images of the indicated soluble or membrane anchored DPR (green), the HIS-58-mCherry nuclear marker (red), and a merged image. Arrows point to nuclear regions defined by the HIS-58 mCherry signal. Coincident green and red signal in the 'TM-(PR)₅₀' image is intestinal autofluorescence. Scale bar = 10 microns. (B) Paralysis assay comparing animals expressing soluble or transmembrane localized (GR)₅₀ (top) or (PR)₅₀ (bottom). N=48-50 animals per genotype, *** - $p < 0.001$, ** - $p < 0.01$, * - $p < 0.05$ (Log-rank test with Bonferroni adjusted p-value). (C) Representative images of HIS-58 anchored (PR)₅₀ (green; top) or unanchored (PR)₅₀ (green; bottom), HIS-58-mCherry nuclear marker (red), and a merged image. Scale bar = 5 microns. (D) Paralysis assay comparing animals expressing nuclear

localized GFP or (PR)₅₀. n≥30 animals per genotype, ** - p<0.01 (Log-rank test with Bonferroni adjusted p-value). (E) Paralysis assay comparing soluble (PR)₅₀ with *his-58*-(PR)₅₀. n≥ 50 animals ((PR)₅₀) or 80 animals (*his-58*-(PR)₅₀), *** - p<0.001 (Log-rank test with Bonferroni adjusted p-value).

Figure 6 – Age-onset toxicity requires continuous DPR expression. (A) Images of worms expressing the indicated DPR under the control of a heat shock inducible promoter. Red fluorescence shows the *myo-3p::mCherry* transgenic marker. Green fluorescence shows the *hsp-16.2p::DPR-GFP* signal. All DPRs are shown 2-4 hours after heat shock. Insets show an enlarged view of the region identified by the dashed boxes. Arrows in the '(GA)₅₀' inset point to putative protein aggregates, suggesting that (GA)₅₀ rapidly aggregates after synthesis. Arrows in the (PR)₅₀ inset point to sites of nuclear localization in the intestine. No such nuclear localization was observed in the (GR)₅₀ line after heat shock. (B) Developmental toxicity of transgenic embryos expressing the indicated *hsp-16.2p::DPR-GFP*. Embryos were heat shocked at 35°C for 30 minutes and then returned to 20°C. The number that reached ≥L4 after 48 hours were scored as 'growth' while the remaining animals were scored as 'no growth'. N≥81 transgenic animals per condition. *** - p<0.001 (Fisher's exact test vs. GFP + H.S.). (C) Adult toxicity of animals expressing either *hsp-16.2p::GFP* or *hsp-16.2p::(PR)₅₀-GFP*. Animals were subjected to either a heat shock (30 minutes, 35°C) on day 1, day 4, or on days 1, 2, 3, and 4. Every 24 hours, animals were scored as either mobile, censored, or affected (paralyzed + dead = '% with phenotype'). Heat shock induction of (GA)₅₀, (PA)₅₀, and (GR)₅₀ produced phenotypes identical to that of GFP. N≥60 animals per

genotype. *** - $p < 0.001$ vs. GFP; days 1-4 H.S. (Log-rank test with Bonferroni adjusted p-value).

Figure 7 – Altering the rate of ageing affects (PR)₅₀ but not (GR)₅₀ toxicity. (A)

Paralysis assay of animals expressing GFP, (GR)₅₀, or (PR)₅₀ under the control of the *myo-3* promoter in the wild type or *daf-2(e1370)* background. ‘Day 0’ animals were isolated as L4 stage animals. N=48-50 animals per genotype. n.s. – ‘not significant’, ** - $p < 0.01$ vs. GFP control (Log-rank test with Bonferroni adjusted p-value). (B) Paralysis assay of animals expressing (PR)₅₀ under the control of the *myo-3* promoter in the wild type, *daf-16(mu86)*, or *daf-2(e1370); daf-16(mu86)* background. N=48-50 animals per genotype. n.s. – ‘not significant’, *** - $p < 0.001$ vs. (PR)₅₀ (Log-rank test with Bonferroni adjusted p-value). (C) Paralysis assay of animals expressing (PR)₅₀ under the control of the *myo-3* promoter in the wild type or *hsf-1(sy441)* mutant background. N=48-50 animals per genotype. *** - $p < 0.001$ vs wild type (Log-rank test with Bonferroni adjusted p-value). (D) Fluorescent microscopy images of day 1 adult worms expressing either (GR)₅₀ or (PR)₅₀ (green) and soluble muscle mCherry (red) in the wild type or *daf-2(e1370)* mutant background. Arrow points to site of nuclear DPR accumulation. Scale bar equals ten microns. (E) Fluorescent microscopy images of day 1 adult worms expressing (PR)₅₀ (green) and soluble muscle mCherry (red) in the *daf-16(mu86)* or *daf-2(e1370); daf-16(mu86)* mutant background. Arrow points to site of nuclear DPR accumulation. Scale bar equals ten microns. (F) Fluorescent microscopy images of day 1 adult worms expressing (PR)₅₀ (green) and soluble muscle mCherry (red) in the wild type

or *hsf-1(sy441)* mutant background. Arrow points to site of nuclear DPR accumulation. Scale bar equals ten microns.

Figure S1 – Lifespan of animals expressing the indicated dipeptide under the control of the *myo-3* promoter. Assays were performed at 25°C. N = 50 animals per genotype. *** - $p < 0.001$ (Log-rank test with Bonferroni adjusted p-value). Table lists lifespan statistics from this experiment.

Figure S2 – Toxic arginine-containing DPRs are not expressed at higher levels than non-toxic DPRs. qPCR of dipeptide mRNA levels in each of the indicated lines. 500 day 1 young adult animals were isolated using a COPAS Biosorter and mRNA was isolated. qPCR was performed using primers directed towards GFP or *act-2* (normalization control). Data are normalized against values from worms expressing GFP only. Data shown are mean \pm S.E.M. N=3. ‘n.s.’ – not significant (One-way ANOVA with Tukey post-hoc test). Raw qPCR data are provided in Table S2.

Figure S3 – The toxicity of arginine-containing DPR-GFP proteins expressed in muscle is not due to higher protein levels. (A) Images of day 1 adult hermaphrodites expressing the indicated *myo-3p::DPR-GFP* protein. Images were acquired using identical exposure settings. (B) COPAS quantification of DPR-GFP levels in the indicated transgenic lines. Data shown are mean \pm S.D. and are normalized to the mean of the GFP control line.

N=42-224 animals. **** - $p < 0.0001$ (One way ANOVA with Dunn's multiple comparisons test.)

Figure S4 - Paralysis assay of animals expressing GFP, (PR)₅₀, or (PR)₅₀ lacking a start ATG codon under the control of the *myo-3* promoter in the wild type background. 'Day 0' animals were isolated as L4 stage animals. N=47-49 animals per genotype. **** - $p < 0.0001$ vs. GFP control (Log-rank test with Bonferroni adjusted p-value).

Figure S5 – The enhanced toxicity of *his-58*-(PR)₅₀ is not due to higher expression levels. COPAS quantification of DPR-GFP levels in the indicated transgenic lines. Data shown are mean \pm S.D. N=53 (PR)₅₀-GFP and 35 (*his-58*-(PR)₅₀). **** - $p < 0.0001$ (2-tailed T-test.)

Figure S6 – The toxicity of induced (PR)₅₀ is not due to higher induction levels. COPAS quantification of DPR-GFP levels in the indicated transgenic lines. Data for each DPR were normalized to the no heat shock control for that strain. Data shown are mean \pm S.D. Numbers at bottom of each bar represent then N for that sample.

Figure S7 – Mutations in the insulin/IGF receptor gene *daf-2* reduce (PR)₅₀-induced neuronal membrane blebbing. Data shown are mean \pm S.D. N=20 for each genotype. ** - $p < 0.01$, **** - $p < 0.0001$, One-way ANOVA, Dunn's multiple comparisons test.

Figure 1

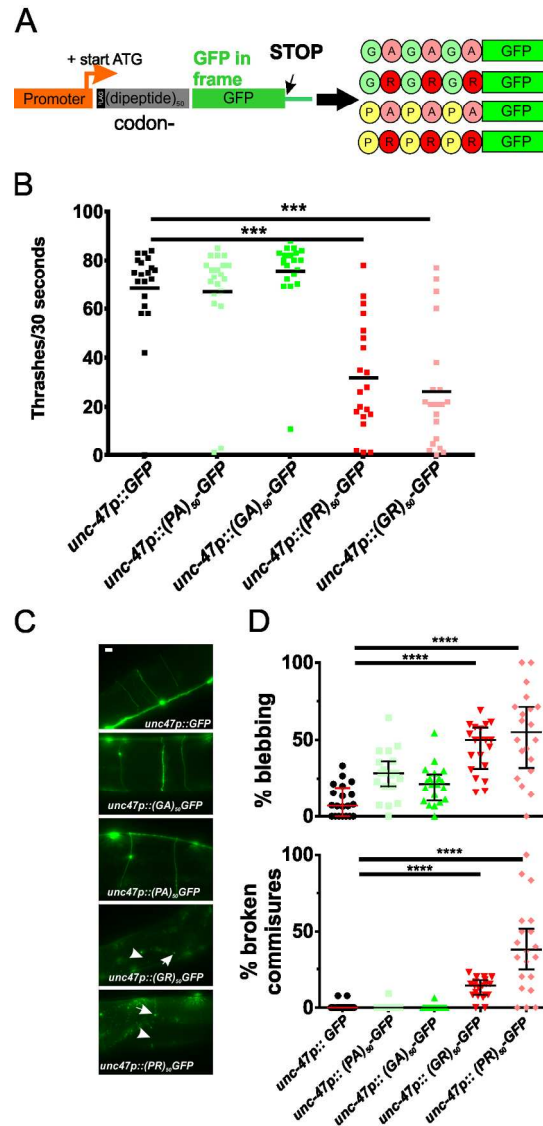


Figure 1 – Arginine-containing DPRs are toxic in motor neurons. (A) Molecular strategy for expression of codon-varied dipeptide repeat proteins in *C. elegans* (B) Liquid thrashing quantification of transgenic animals expressing the indicated DPR under the motor neuron-specific *unc-47* promoter. N=20 animals per genotype. Each symbol represents quantification for one animal, horizontal line indicates population median. *** - $p < 0.001$ vs GFP control, (One-way non-parametric ANOVA with Dunn's post-hoc test). (C) Representative images of *unc-47+* motor neurons in animals expressing the indicated DPR. Arrowheads point to an example of membrane blebbing. Arrowhead points to examples of commissure breaks. Scale bar = 10 microns (D) Quantification of membrane blebbing and commissure breaks in each of the indicated strains. For each animal, we counted the total number of commissures with blebbing or breaks and divided by the total number of detectable commissures. N=20 animals per genotype. Each symbol represents quantification for one animal expressed as a percentage. The horizontal line indicates population median with interquartile range. **** - $p < 0.0001$ vs GFP control (One-way non-parametric ANOVA with Dunn's post-hoc test). N=20 animals per genotype.

106x235mm (300 x 300 DPI)

Figure 2

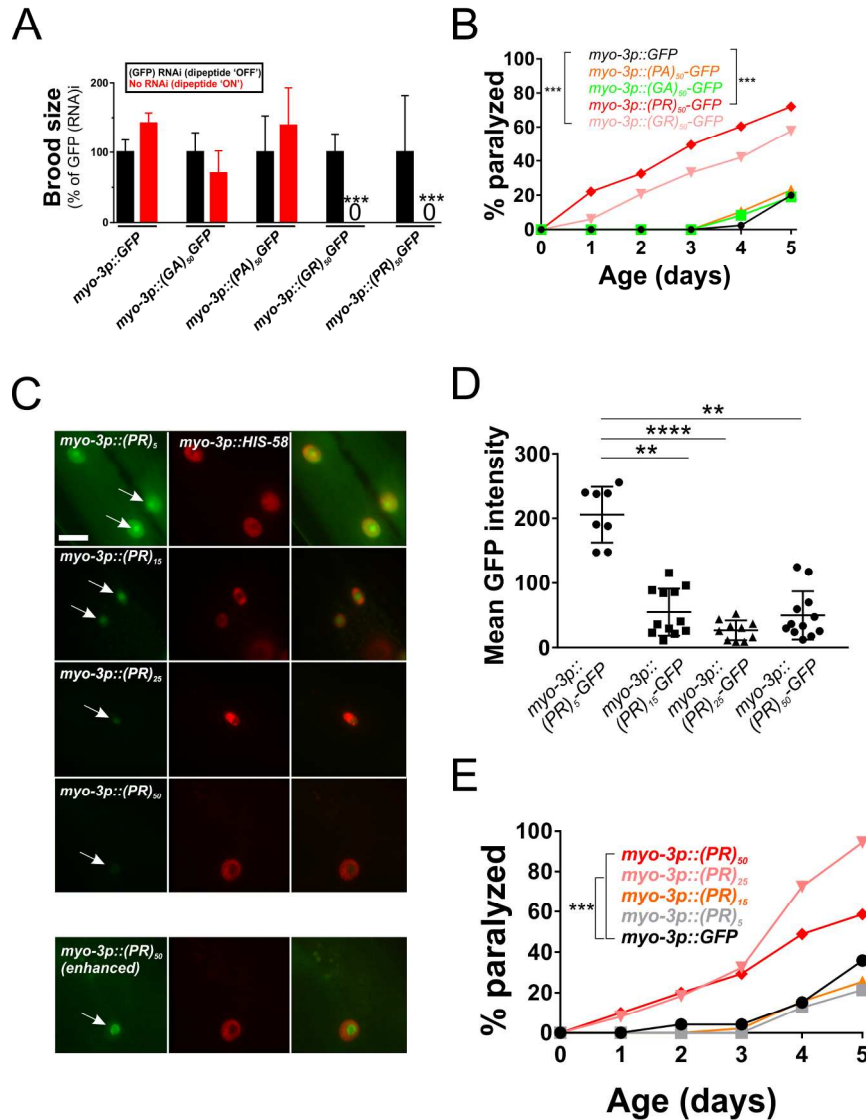


Figure 2 – Muscle expressed arginine-containing dipeptides are toxic in *C. elegans* (A) Brood size for worms expressing each integrated dipeptide protein in the presence or absence of *gfp(RNAi)* at 25°C. Data for each strain are normalized to the mean brood size of animals grown on *gfp(RNAi)*. *** - $p < 0.001$ (One-way ANOVA with post-hoc Tukey test). Raw brood size data for 25°C are included in 'Table S1'. (B) Paralysis assay for adult animals raised in the absence of *gfp(RNAi)*. $N \geq 43-49$ animals per genotype. *** - $p < 0.001$ (Log-rank test with Bonferroni adjusted p-value), (C) Fluorescent microscopy of Day 1 adult hermaphrodites expressing (PR)₅-GFP, (PR)₁₅-GFP, (PR)₂₅-GFP, or (PR)₅₀-GFP (green) in the muscle. Muscle DNA (marked by a *myo-3p::his-58-mCherry* reporter) is in red. Arrows point to sites of nuclear GFP puncta. Scale bar = 10 microns. All images were acquired using identical exposure settings. The row labeled '*myo-3p:::(PR)₅₀ (enhanced)*' was adjusted for brightness and contrast in the GFP channel differently from the other images so that the (PR)₅₀-GFP signal is observable. (D) Quantification of the GFP levels from the indicated PR repeat animals. Each point shows the measured value for a single nucleus, horizontal line indicates population median with interquartile range. ** - $p < 0.01$, **** - $p < 0.0001$ vs GFP control, (One-way non-

parametric ANOVA with Dunn's post-hoc test). (E) Paralysis assay of animals expressing the indicated number of (PR) repeats under the control of the *myo-3* promoter. 'Day 0' animals were isolated as L4 stage animals. N=48-50 animals per genotype. *** - $p < 0.001$ vs. GFP control (Log-rank test with Bonferroni adjusted p-value).

174x228mm (300 x 300 DPI)

Figure 3

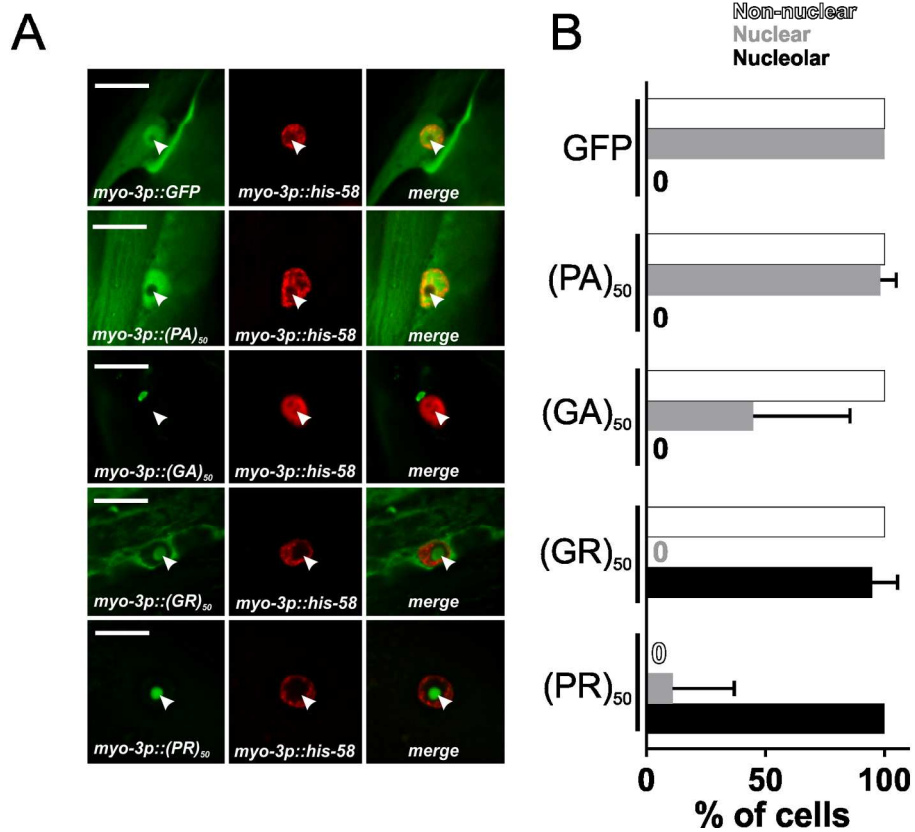


Figure 3 – (PR)₅₀ and (GR)₅₀ are localized to the nucleolus in *C. elegans* muscle cells (A) Imaging of live, anesthetized day 1 adult *C. elegans* hermaphrodites expressing the indicated dipeptide. Green shows dipeptide-GFP localization expressed in muscle, red shows histone-tagRFP within the muscle nucleus. Arrowhead points to the histone-free nucleolar region. Scale bar – 10 microns. (B) Quantification of DPR-GFP signal that is observed in nucleoplasm, nucleolus, and non-nuclear cellular compartments. N=55-78 nuclei from 5-6 animals. Data shown are means \pm S.D.

166x167mm (300 x 300 DPI)

Figure 4

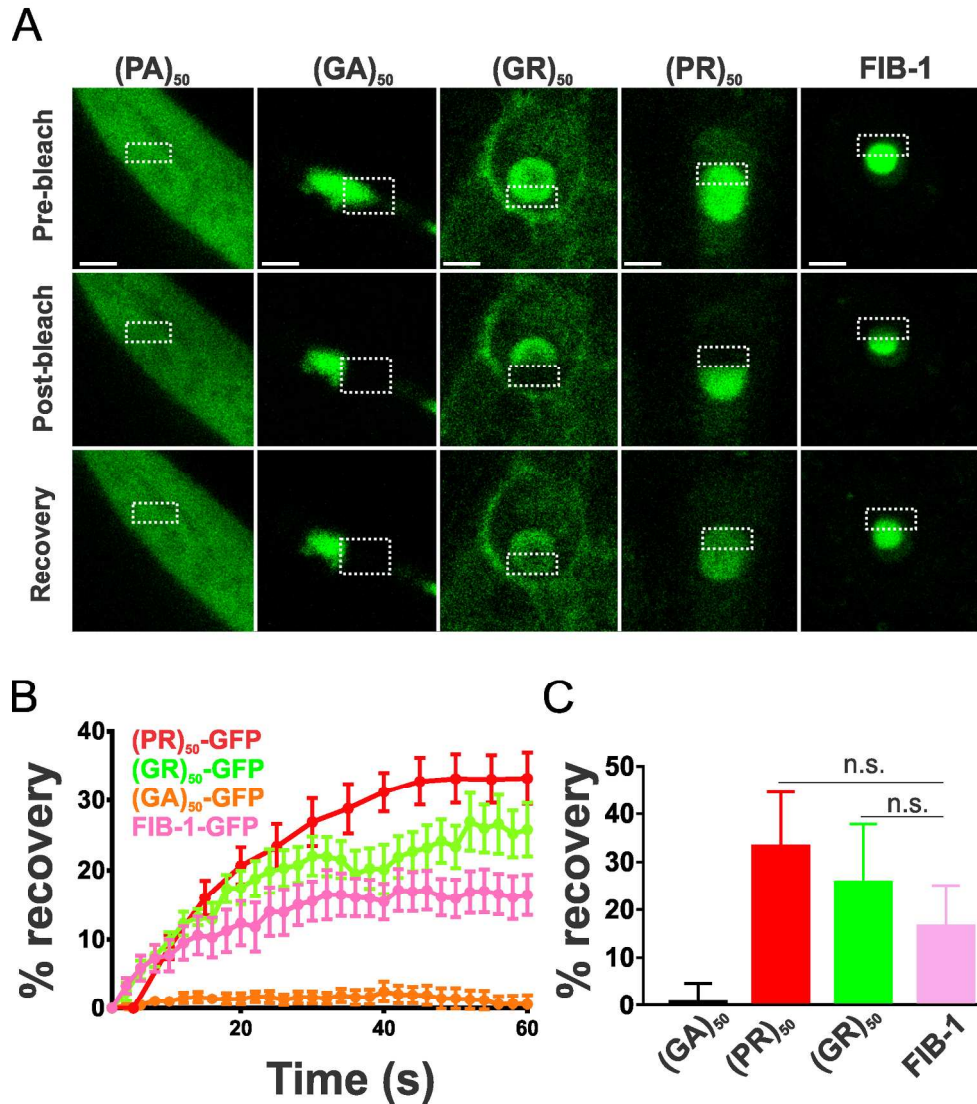


Figure 4 – Arginine-containing DPRs are not aggregates (A) Representative images from FRAP analysis of subcellular localized DPR proteins expressed in muscle. Dashed outline indicates site of photobleaching and post-bleaching quantification. Recovery images are 150 seconds post-bleach. Scale bar = 2 microns (B) Quantification of FRAP imaging. Data shown are mean \pm S.E.M. from 9-10 data sets per genotype. (C) Average equilibrium fluorescence recovery after 60 seconds. Data shown are mean \pm S.D. from 9-10 data sets per genotype. n.s. vs FIB-1-GFP (One-way ANOVA with Dunn's multiple comparison test).

190x220mm (300 x 300 DPI)

Figure 5

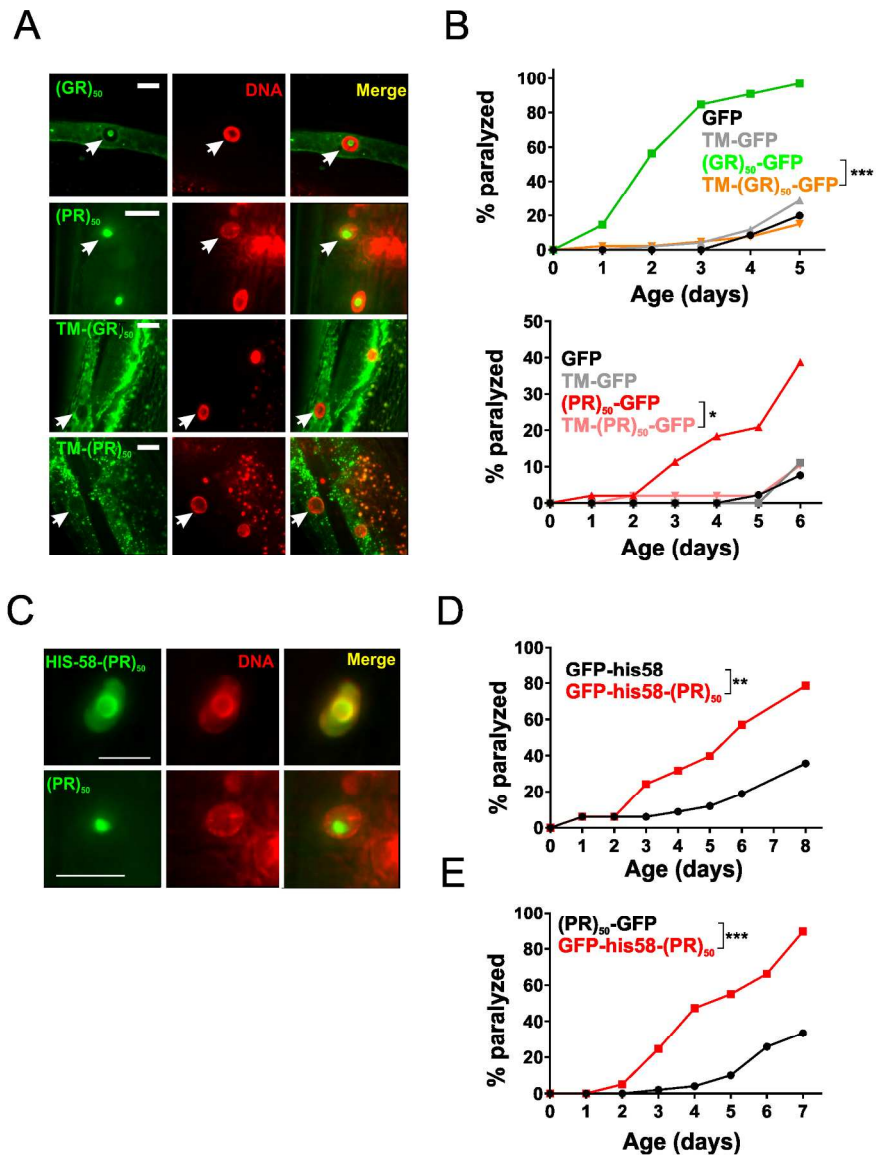
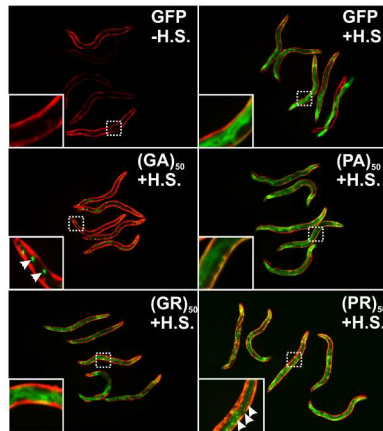


Figure 5 – Nuclear localization of muscle expressed arginine-containing DPRs is necessary and sufficient for toxicity. (A) Representative images of the indicated soluble or membrane anchored DPR (green), the HIS-58-mCherry nuclear marker (red), and a merged image. Arrows point to nuclear regions defined by the HIS-58 mCherry signal. Coincident green and red signal in the 'TM-(PR)50 image is intestinal autofluorescence. Scale bar = 10 microns. (B) Paralysis assay comparing animals expressing soluble or transmembrane localized (GR)50 (top) or (PR)50 (bottom). N=48-50 animals per genotype, *** - $p < 0.001$, ** - $p < 0.01$, * - $p < 0.05$ (Log-rank test with Bonferroni adjusted p-value). (C) Representative images of HIS-58 anchored (PR)50 (green; top) or unanchored (PR)50 (green; bottom), HIS-58-mCherry nuclear marker (red), and a merged image. Scale bar = 5 microns. (D) Paralysis assay comparing animals expressing nuclear localized GFP or (PR)50. $n \geq 30$ animals per genotype, ** - $p < 0.01$ (Log-rank test with Bonferroni adjusted p-value). (E) Paralysis assay comparing soluble (PR)50 with his-58-(PR)50. $n \geq 50$ animals ((PR)50) or 80 animals (his-58-(PR)50), *** - $p < 0.001$ (Log-rank test with Bonferroni adjusted p-value).

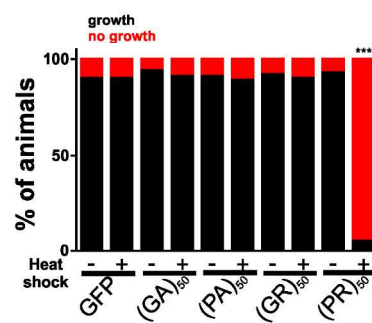
187x256mm (300 x 300 DPI)

Figure 6

A



B



C

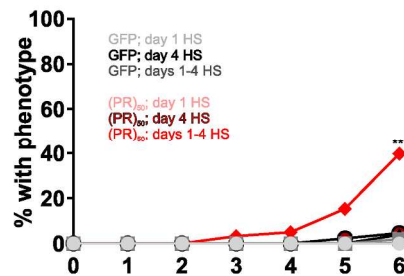


Figure 6 – Age-onset toxicity requires continuous DPR expression. (A) Images of worms expressing the indicated DPR under the control of a heat shock inducible promoter. Red fluorescence shows the myo-3p::mCherry transgenic marker. Green fluorescence shows the hsp-16.2p::DPR-GFP signal. All DPRs are shown 2-4 hours after heat shock. Insets show an enlarged view of the region identified by the dashed boxes. Arrows in the (GA)₅₀ inset point to putative protein aggregates, suggesting that (GA)₅₀ rapidly aggregates after synthesis. Arrows in the (PR)₅₀ inset point to sites of nuclear localization in the intestine. No such nuclear localization was observed in the (GR)₅₀ line after heat shock. (B) Developmental toxicity of transgenic embryos expressing the indicated hsp-16.2p::DPR-GFP. Embryos were heat shocked at 35°C for 30 minutes and then returned to 20°C. The number that reached ≥L4 after 48 hours were scored as 'growth' while the remaining animals were scored as 'no growth'. N≥81 transgenic animals per condition. *** - p<0.001 (Fisher's exact test vs. GFP + H.S.). (C) Adult toxicity of animals expressing either hsp-16.2p::GFP or hsp-16.2p:(PR)₅₀-GFP. Animals were subjected to either a heat shock (30 minutes, 35°C) on day 1, day 4, or on days 1, 2, 3, and 4. Every 24 hours, animals were scored as either

mobile, censored, or affected (paralyzed + dead = '% with phenotype'). Heat shock induction of (GA)50, (PA)50, and (GR)50 produced phenotypes identical to that of GFP. $N \geq 60$ animals per genotype. *** - $p < 0.001$ vs. GFP; days 1-4 H.S. (Log-rank test with Bonferroni adjusted p-value).

151x271mm (300 x 300 DPI)

Figure 7

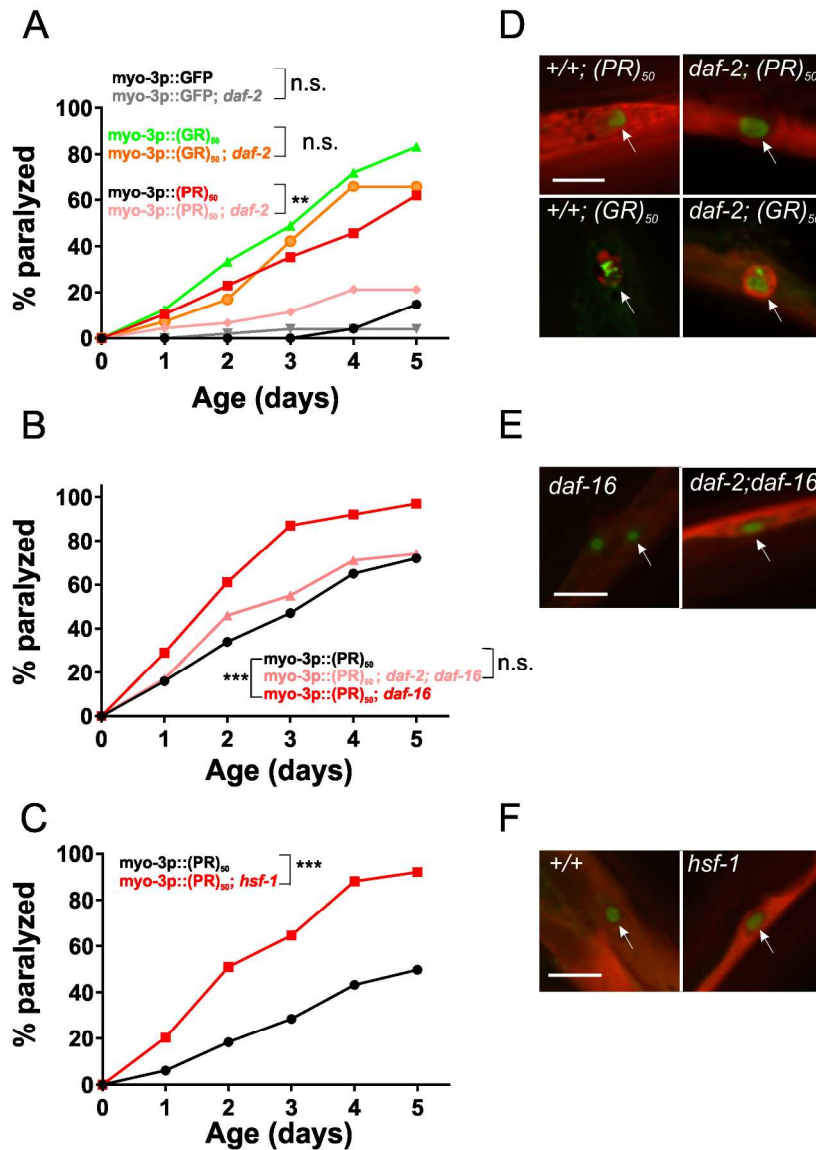


Figure 7 – Altering the rate of ageing affects (PR)50 but not (GR)50 toxicity. (A) Paralysis assay of animals expressing GFP, (GR)50, or (PR)50 under the control of the myo-3 promoter in the wild type or *daf-2*(e1370) background. ‘Day 0’ animals were isolated as L4 stage animals. N=48-50 animals per genotype. n.s. – ‘not significant’, ** - $p < 0.01$ vs. GFP control (Log-rank test with Bonferroni adjusted p-value). (B) Paralysis assay of animals expressing (PR)50 under the control of the myo-3 promoter in the wild type, *daf-16*(mu86), or *daf-2*(e1370); *daf-16*(mu86) background. N=48-50 animals per genotype. n.s. – ‘not significant’, *** - $p < 0.001$ vs. (PR)50 (Log-rank test with Bonferroni adjusted p-value). (C) Paralysis assay of animals expressing (PR)50 under the control of the myo-3 promoter in the wild type or *hsf-1*(sy441) mutant background. N= 48-50 animals per genotype. *** - $p < 0.001$ vs wild type (Log-rank test with Bonferroni adjusted p-value). (D) Fluorescent microscopy images of day 1 adult worms expressing either (GR)50 or (PR)50 (green) and soluble muscle mCherry (red) in the wild type or *daf-2*(e1370) mutant background. Arrow points to site of nuclear DPR accumulation. Scale bar equals ten microns. (E) Fluorescent microscopy images of day 1 adult worms expressing (PR)50 (green) and soluble muscle

mCherry (red) in the *daf-16(mu86)* or *daf-2(e1370); daf-16(mu86)* mutant background. Arrow points to site of nuclear DPR accumulation. Scale bar equals ten microns. (F) Fluorescent microscopy images of day 1 adult worms expressing (PR)50 (green) and soluble muscle mCherry (red) in the wild type or *hsf-1(sy441)* mutant background. Arrow points to site of nuclear DPR accumulation. Scale bar equals ten microns.

183x263mm (300 x 300 DPI)